PERGAMON

International Journal of Solids and Structures 39 (2002) 709–723

INTERNATIONAL JOURNAL OF SOLIDS and STRUCTURES

www.elsevier.com/locate/ijsolstr

Wrinkling of tubes in bending from finite strain three-dimensional continuum theory

Ralf Peek *

Shell Global Solutions International, OGUP, Room S-5024, Postbus 60, 2280 AB Rijswijk, The Netherlands

Received 9 April 2000; received in revised form 20 March 2001

Abstract

The problem of a tube under pure bending is first solved as a generalised plane strain problem. This then provides the prebifurcation solution, which is uniform along the length of the tube. The onset of wrinkling is then predicted by introducing buckling modes involving a sinusoidal variation of the displacements along the length of the tube. Both the prebuckling analysis and the bifurcation check require only a two-dimensional finite element discretisation of the cross-section with special elements. The formulation does not rely on any of the approximations of a shell theory, or small strains. The same elements can be used for pure bending and local buckling a prismatic beam of arbitrary cross-section. Here the flow theory of plasticity with isotropic hardening is used for the prebuckling solution, but the bifurcation check is based on the incremental moduli of a finite strain deformation theory of plasticity.

For tubes under pure bending, the results for limit point collapse (due to ovalisation) and bifurcation buckling (wrinkling) are compared to existing analysis and test results, to see whether removing the approximations of a shell theory and small strains (used in the existing analyses) leads to a better prediction of the experimental results. The small strain analysis results depend on whether the true or nominal stress–strain curve is used. By comparing small and finite strain analysis results it is found that the small strain approximation is good if one uses (a) the nominal stress–strain curve in compression to predict bifurcation buckling (wrinkling), and (b) the true stress–strain curve to calculate the limit point collapse curvature.

In regard to the shell theory approximations, it is found that the three-dimensional continuum theory predicts slightly shorter critical wrinkling wavelengths, especially for lower diameter-to-wall-thickness (D/t) ratios. However this difference is not sufficient to account for the significantly lower wavelengths observed in the tests.

Keywords: Three-dimensional; Bending; Strain

1. Introduction

Circumstances under which a pipe or tube will be subjected to plastic bending deformations in the course of hydrocarbon exploration and production activities include coiled tubing operations, offshore pipeline

* Tel.: +31-70-311-3554; fax: +31-70-311-3510.
E-mail address: r.peek@siep.shell.com (R. Peek).

0020-7683/02/$ - see front matter
PII: S0020-7683(01)00091-9

installation by reeling, pulling of the pipe through a J-tube, laying the pipe on an uneven seabed, or cold-bending of pipe joints for onshore installation. During such operations plastic bending deformations are acceptable, and even intended. However localised buckling or wrinkling are not acceptable.

There are two ways in which unacceptable deformations can develop in a tube under plastic bending (Jirsa et al., 1972; Reddy, 1979; Kyriakides and Ju, 1992): buckling due to ovalisation occurs when the loss of moment capacity due to increasing ovalisation can no longer be offset by the strain hardening of the material. This causes the moment for a pipe under uniform bending to reach a maximum value (limit point). Beyond the limit point, the deformations tend to localise rapidly. For thinner walled pipes, wrinkling occurs before buckling due to ovalisation. This involves wavy deformations forming on the compression side of the pipe, which grow under increasing curvature and initially increasing bending moment, and then localise. The initial formation of such wrinkles is a symmetry breaking bifurcation, from a prebuckling state for which conditions are constant all along the length of the pipe to one which involves ripples developing on the compression side of the pipe.

A small increment in bending deformation is generally possible from the point of incipient wrinkling (bifurcation) until localisation of the deformations in an unacceptable way (Kyriakides and Ju, 1992). This means that the pipe may be bent slightly beyond the bifurcation strain. For design purposes, however, it is prudent to neglect this extra bit of deformation capacity. [1] As a result the critical bending deformation is the lesser of the deformations at the limit and bifurcation points.

Of a number of experimental and analytical investigations of the behaviour of tubes under bending (Jirsa et al., 1972; Reddy, 1979; Murphy and Langner, 1985; Bai et al., 1995; Kyriakides and Ju, 1992; Ju and Kyriakides, 1992), the one involving perhaps the most incisive comparison of experimental and analysis results is the one of Kyriakides and Ju. They obtained excellent agreement between the experimental and analytical values of the critical bending deformations, by performing very carefully controlled and monitored experiments, as well as measuring all the relevant properties needed for input into the analysis. Their analysis includes the prebuckling solution (uniform along the length of the pipe), as well as a bifurcation check (to determine the point at which wrinkling deformations start to develop and the critical wrinkling wavelength), and even postbifurcation analysis. Their analyses are valid for finite rotations, but employ the approximations of small strains, and the theory of thin shells.

Despite the excellent agreement between the experimental critical bending strains of Kyriakides and Ju with their predictions, such excellent agreement was not observed for all parameters: for the wavelength of the wrinkling mode, the experimental values ranged from 50% to 90% of the predicted ones. There is also a slight difference in the cross-over point. That is the point where the failure mode changes from (limit point) buckling due to ovalisation to (bifurcation) wrinkling: with the cross-over point being at $D/t = 22$ for the analysis around $D/t = 26$ for the experiments.

In view of the differences in the wrinkling wavelengths, it is of interest to investigate to what extent these may be influenced by the approximations of small strains, and the theory of thin shells in the analysis of Kyriakides and Ju. For this purpose, the analysis is repeated here without relying on the small strain and shell theory approximations. The results are compared to the analysis and test results of Ju and Kyriakides, to determine the significance of these effects, and to see to what extent they affect the differences between analysis and experimental results.

The nomenclature used in the main body of this paper are defined below. For the appendix, an independent nomenclature is used, with symbols defined where they are first used.

[1] Indeed due to imperfections such as those that can arise due to misalignment offset at girth welds the actual deformation capacity of the imperfect pipe can fall considerably below that of a perfect pipe (Yoosef-Ghodsi et al., 1994; Souza and Murray, 1994). Such imperfections are not considered in this paper, however.

D outer pipe diameter
L half wavelength of the critical wrinkling mode
t wall thickness

The "nominal bending strain" means the curvature of the pipe multiplied by one half the undeformed outer diameter of the pipe. (Due to ovalisation, this is somewhat larger than then actual axial strain at the extreme fibres.)

2. Analysis methodology

Details of the analysis methodology are given in the appendix. It is based on the finite strain constitutive theory quoted in Needleman and Tvergaard (1977), with the J_2 flow theory of plasticity being used for the prebuckling solution, and the J_2 deformation theory for the bifurcation check. This approach based on the flow and deformation theories has also been used by Kyriakides and Ju (1992), and is generally known to give bifurcation buckling predictions that are in better agreement with experimental results (Batdorf, 1949; Sanders, 1954; Christofersen and Hutchinson, 1979; Bushnell, 1982; Needleman and Tvergaard, 1982; Tvergaard, 1983; Blachut et al., 1996).

The generalised plane strain (GPE) formulation used here for the prebuckling solution is not new (Cook, 1989; HKS, 1989; Boussaa et al., 1995, 1996). Essentially it corresponds to a model of a thin slice of the pipe confined between ideally lubricated plates that can transmit tensile or compressive stresses, but no shear stresses. This slice model represents a pipe in uniform bending. As a result only the cross-section needs to be discretised. For this a uniform mesh consisting of 7 elements across the wall thickness by 300 elements around the half circumference (to make for a total of 2100 elements) is used. The elements are 4-noded isoparametric quadrilateral GPE elements with a single integration point, and hourglass control according to the formulation of Belytschko and Ong (1984). These GPE elements have an additional (5th) node, for which the degrees of freedom represent the curvature and overall axial deformation of the pipe. Any bending moment and/or axial force acting on the pipe is applied to this extra node.

For the bifurcation check, buckling modes that involve sinusoidal variations of the displacements along the length of the pipe are introduced. The critical wavelength of these buckling modes is the one for which bifurcation is first detected. Although formulations that also combine sinusoidal variations for the buckling modes in one of the coordinate directions with a finite element type discretisation in for the other coordinate have been used in the context of plate and shell theories (Tang et al., 1985), this appears to be the first formulation and implementation of such an approach for finite strain GPE elements. More information on this formulation is given in the appendix.

Avoiding the shell theory and small strain approximations is not the only advantage of the GPE formulation described. It is also an approach that is readily coded if one starts from an existing finite element code with plane strain element, and existing routines for finite strain computations. This is true for the bifurcation check as well as the prebuckling solution. It is essentially a plane-strain-like element including just a few extra terms.

This GPE formulation with a bifurcation check is not only applicable to tubes, but also to any other cross-sectional shape. For instance one could use the same formulation to predict the buckling of the flanges of a structural I-beam, of plate girders or even of an airplane wing structure of uniform cross-section. This versatility of the formulation also creates the possibility to verify it against problems for which published results are available.

Perhaps the simplest large strain bifurcation under pure bending problem is that of bending of a plate. For this Triantafyllidis (1980) has shown that the critical bifurcation mode is a surface instability mode on the compression side. The methodology applied here yielded the same prediction of a surface instability

mode, and a critical curvature that agreed with that of Triantafyllidis to within the accuracy that the result could be scaled from Triantafyllids' paper.

Another large strain bifurcation problem against which the formulation could be verified is that of necking of a thin sheet. With the formulation developed here, this problem can be solved with a small number of elements, even when the critical angle at which the band of localised deformation will form is not known a priori. Indeed the analysis can be set up in such a way that the critical wavelength for the bifurcation mode provides this angle. This gives results for the orientation of the band and the critical strains that are in excellent agreement with the analytical ones from Stören and Rice (1975), if the sheet is taken to be sufficiently thin compared to the possible bifurcation wavelengths, and a high value of Young's modulus is chosen to match the rigid-plastic approximation of Stören and Rice's analytical solution.

Although the above verification problems suggest that the method developed also is useful for the study of bifurcation problems in metal forming, the objective here is to focus on predictions for the bending of tubes, and the extent to which these may be influenced by finite strain effects, or the approximations of shell theory. For this purpose it is first necessary to clearly define what stress–strain curves are used in the finite strain analyses, and how these relate to the stress–strain curves used in the small strain analyses.

3. Matching of stress–strain curves for small and finite strain analyses

In their analyses, Kyriakides and Ju use a Ramberg–Osgood stress–strain relation in the form

$$\varepsilon = \frac{\sigma}{E}\left[1 + \frac{3}{7}\left(\frac{\sigma}{\sigma_y}\right)^{n-1}\right] \tag{1}$$

in which $E = 10^4$ ksi (68.95 GPa), $\sigma_y = 42.6$ ksi (293.7 MPa), and $n = 29$. These represent the "average values" of the material parameters from a number of "uniaxial tests on axial specimens". From the description provided, it is not fully clear to which stress and strain measures Eq. (1) applies. For this three possibilities are considered here:

1. taking Eq. (1) to be the nominal stress–strain relationship in tension,
2. taking Eq. (1) to be the true stress–strain relationship, and
3. taking Eq. (1) to be the nominal stress–strain relationship in compression.

Here the term "nominal stress–strain relationship" is used here to describe the relationship between nominal stress and engineering strain, and "true stress–strain relationship" is used to describe the relationship between true stress and logarithmic strain.

From the three cases considered, the implied true stress–strain relationship is the steepest for case (1) and the flattest for case (3). Thus the highest predictions of buckling and wrinkling strains from the finite strain analysis can be expected for case (1) and the lowest for case (3). These predictions are given in the following section, together with the small strain and experimental results of Kyriakides and Ju.

4. Results

The results for the critical bending strains are shown in Figs. 1–3. Specifically, the nominal bending strain at the limit point (point of maximum bending moment assuming that no wrinkling deformations develop) is plotted in Fig. 1, the incipient wrinkling (bifurcation) strain in Fig. 2, and Fig. 3 shows the smallest of these two critical strains for each value of D/t, as well as the cross-over points, where the predicted strains

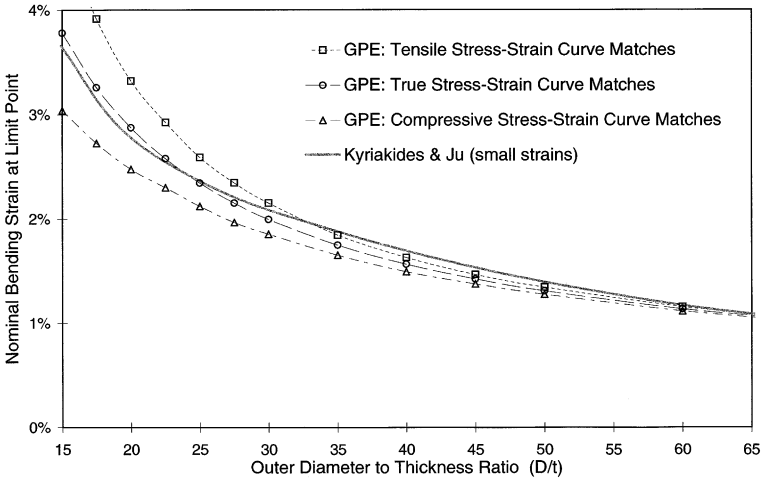

Fig. 1. Comparison of calculated strains for (limit point) buckling due to ovalisation from the method developed (based on finite strain continuum theory) with that from Kyriakides and Ju (based on small strains, and use of a shell theory).

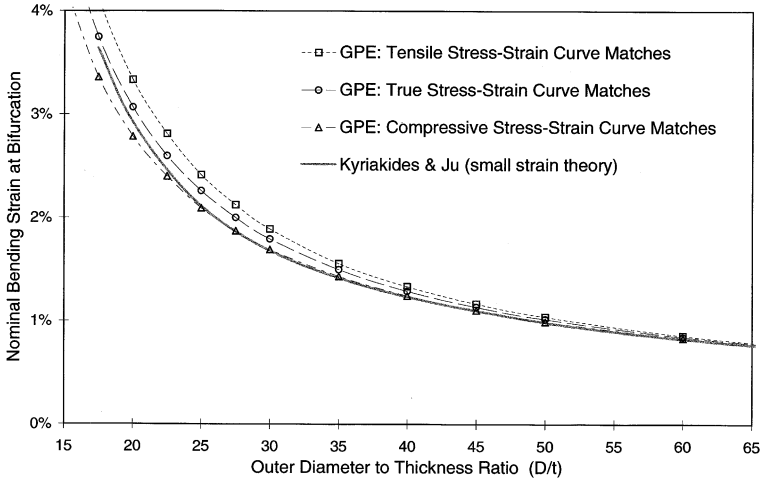

Fig. 2. Comparison of calculated strains for incipient wrinkling (bifurcation) from the method developed (based on finite strain continuum theory) with that from Kyriakides and Ju (based on small strains, and use of a shell theory).

for (limit point) buckling due to ovalisation coincide with those for (bifurcation) wrinkling as solid black triangles. To the left of the cross-over point (smaller D/t) the failure mode is buckling due to ovalisation, whereas to the right (larger D/t) it is wrinkling. The experimental observations of buckling due to ovalisation and wrinkling from Kyriakides and Ju (1992) are also shown in Fig. 3 as circles and crosses respectively. These figures lead to the following observations and explanations:

1. From Fig. 1, in the range $15 < D/t < 25$, strains for buckling due to ovalisation from the small strain (Kyriakides and Ju, 1992) and finite strain (GPE) analyses are in good agreement when the stress–strain curve for the small strain analysis is the true stress–strain relation. This is not surprising since the uniform bending stiffness depends on both the stiffness in tension (which is overestimated by the true stress–strain

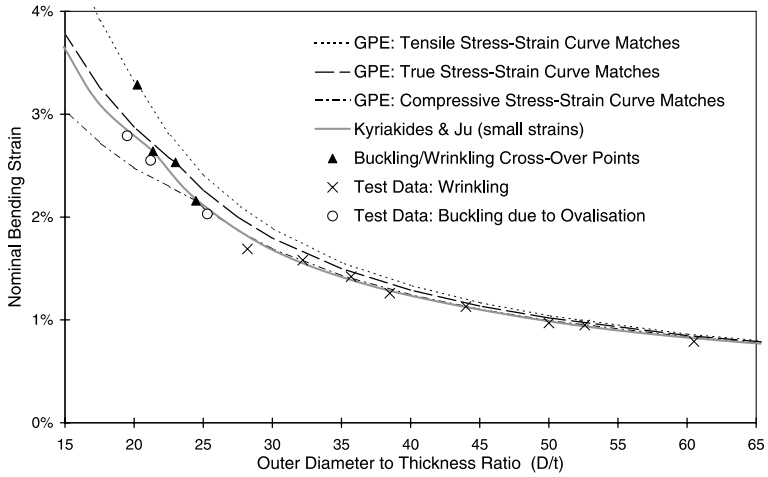

Fig. 3. Comparison of calculated critical strains (defined as the limit point or bifurcation strain, whichever is smallest) with experimental results from Kyriakides and Ju.

relation) and the stiffness in compression (which is underestimated by the true stress–strain relation), so that the errors from the small strain approximation from the tension and compression side balance out for this case.

2. From Fig. 1, for $D/t > 25$, the small strain analysis predicts generally higher limit point strains. Although the reason for this is not clear (it could be due to discretisation errors), [2]. it is also not so important, since in this range failure is by wrinkling rather than by (limit point) buckling due to ovalisation.

3. Regarding the incipient wrinkling (bifurcation) strains of Fig. 3, for $D/t > 25$, the small strain results coincide almost exactly with the finite strain results, when the stress–strain curve used in the small strain analysis is the nominal stress–strain curve in compression. This is also not surprising, since wrinkling occurs in the compression region so that the stiffness of the material in compression is most relevant. Similar observations have been made comparing Batterman's (Batterman, 1965, 1967) small strain result for axisymmetric wrinkling for a tube under axial loading, with a finite strain version of the same result (Peek, 2000).

4. In the above observations it has been assumed that any differences between the Ju and Kyriakides analyses and the present one is due to the small strain approximation, and not due to the approximations of the shell theory. The effects of the shell theory approximation become more apparent in Fig. 2, for $D/t < 25$, where the small strain result rises above the finite strain result based on matching the compressive stress–strain curve. Here the wrinkling wavelengths become smaller compared to the wall thickness, so that errors due to the approximations of the shell theory start to become noticeable.

5. When comparing the critical bending strains from the experiments and the analyses in Fig. 3, it is seen that the Kyriakides and Ju results fit the experimental data slightly better than any of the finite strain analyses. Specifically, if the finite strain analysis is based on matching the compressive stress–strain curve, the (limit point) ovalisation buckling strains are underestimated slightly compared to the test data, and if the finite strain analysis is based on matching the true stress–strain curve, it overestimates the critical strains

[2] The moment curvature diagram is typically quite flat at the limit point, so that a small difference in apparent stiffness can make a much more significant difference in the bending strain at which the maximum moment (limit point) occurs.

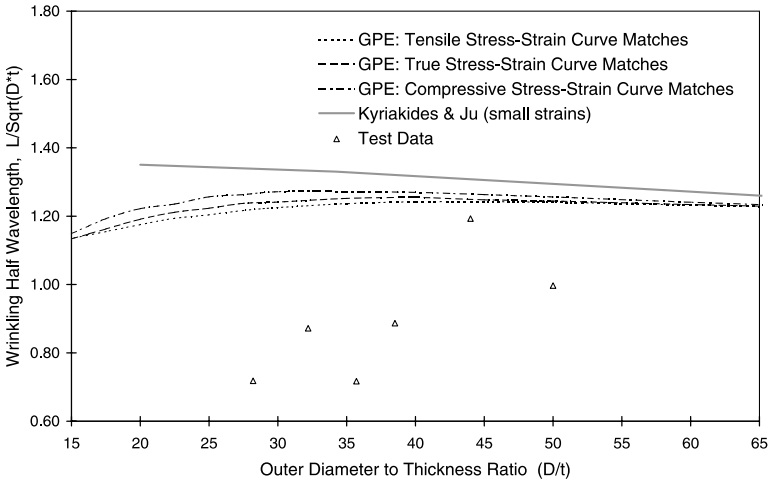

Fig. 4. Comparison of calculated critical wrinkling wavelengths with experimental results from Kyriakides and Ju.

slightly in the (bifurcation) wrinkling region. Paradoxically, despite this, the present analysis gives a better prediction of the limit-point-to-bifurcation cross-over point. Generally the differences being examined here are quite small. They could be due to other factors, such as variability in the stress–strain curves. It must also be remembered both the small and finite strain plasticity theories, represent rather idealised views of multiaxial material behaviour, when compared to experimental observations such as those collected in Hecker (1976).

Finally the half wavelengths of the critical bifurcation modes are shown in Fig. 4. Here the agreement with the experimental results improves slightly, when one does not rely on the approximations of thin shells or small deformations. However the predictions are still significantly higher than the experimental observations of the buckling wavelength. The reasons for this are not clear. Certainly the behaviour of metals under multiaxial and non-proportional loading is quite complex (Hecker, 1976). It is certainly conceivable that the relatively simple material idealisation used provides good predictions of one parameter (the critical strain), but not of another.

5. Closing remarks

For plastic bending of the aluminum tubes considered here, it is clear that the approximations of thin shell theory and small strains are good. In this case, the finite strain three-dimensional continuum analysis presented here could be considered an optional refinement. It does improve the predictions of the buckling wavelengths, but not sufficiently to account for the differences between analysis and experiment. Thus some other phenomenon must be responsible for the shorter buckling wavelengths from the experiments. In view of the care taken in the experimental work, and any questions regarding geometric/kinematic approximations made in the analysis now being removed, the only reasonable explanation for the discrepancy in the wrinkling wavelengths is that the real material response under non-proportional loading that differs from the idealisation used based on the J_2 deformation and flow theories of plasticity.

For some materials, the stress–strain curves become very flat at low strains. Finite strain effects then also play a role at lower strains. For instance in tensile coupon tests on longitudinal specimen taken from some 13% Cr stainless steel pipes, the ultimate (i.e. maximum load) condition is reached at strains as low as 2%.

Using this same stress–strain curve [3] for the finite element calculations of the critical bending strains, yields limit and bifurcation strains larger than the ultimate value of 2%, for sufficiently thick-walled pipes in bending. This not only indicates no wrinkling on the compression side until beyond ultimate, but also no necking on the tension side of the bent pipe. Just like wrinkling, incipient necking is also detected as a bifurcation when using the GPE elements described here. Clearly it would not make sense to attempt this sort of prediction relying on the theory of thin shells with small strains.

Appendix A. Formulation of generalised plane strain finite element with bifurcation check

The analyses reported in this paper are based on (a) a prebuckling solution based on a GPE formulation, and (b) a bifurcation check that includes wrinkling-type modes involving a sinusoidal variation in the axial direction. The formulation presented here is applicable for straight or curved beams of arbitrary cross-section, provided that the prebuckling solution involves conditions that are constant from one cross-section to the next along the length of the beam. For this reason the term "beam" is used in this appendix rather than "pipe". In this context a pipe is merely a special case of a beam. Axial loads and internal pressure or other uniform loads can also be introduced, provided a provision is made by the nodal boundary conditions to generate the required reactions to such loads while maintaining constant conditions along the length of the pipe. (For instance an axial load must be accompanied by a transverse reaction equal to the axial load divided by the radius of curvature in the deformed configuration.)

Although the GPE formulation for prebuckling is not new (Cook, 1989; HKS, 1989; Boussaa et al., 1995, 1996), it is briefly outlined here to set the scene for the formulation of the bifurcation analysis, involving buckling modes with a sinusoidal variation along the length of the beam.

A.1. Prebuckling deformation kinematics

Consider a beam of arbitrary, but constant cross-section consisting of a number of material fibres running along the length of the beam (i.e. normal to the cross-sections). The deformation of the beam is assumed to occur in a fixed plane of deformation, such that all fibres remain parallel to this plane of deformation. A coordinate x is measured normal to the plane of deformation, and the unit normal vector to the plane of deformation is denoted by $\mathbf{t}_x$.

Within the plane of deformation a reference line is defined of length l, and uniform curvature θ/l where θ is the rotation of one end of the reference line with respect to the other. Thus the reference line is a segment of a circle, lying in the plane of deformation. One of the ends of the reference line will be labelled "the beginning" and the "the end". A unit vector tangent to the reference line and pointing from its beginning towards its end is denoted by $\mathbf{t}_z$. The angle θ is taken to be positive whenever the unit vector $\mathbf{t}_z$ undergoes positive rotation about the x axis (in the sense of the right-hand rule) as one moves from the beginning towards the end of the reference line. The length of the reference line l and its bend angle θ may vary as a function of time. This is indicated by the notation,

$$l = l(t), \quad \theta = \theta(t), \tag{A.1}$$

where t denotes time. Thus the position of the reference line changes in time. For simplicity, however, the position and orientation of the beginning of the reference line will be taken to be fixed in space. (There is no loss of generality in this, since rigid body motions can always be applied and do not change the state of

[3] Up to ultimate, a piecewise linear representation based on the actual values recorded during the coupon test is used. Beyond ultimate, a Ramberg–Osgood power law relationship between the true stress and logarithmic plastic strain is used to extend the stress–strain relationship with the parameters of the power law chosen to match the stress and tangent moduli at ultimate.

deformation or stress.) Let $\mathbf{t}_z(\alpha)$ be a unit vector obtained by rotating the tangent to the reference line at its beginning by an angle α about the x-axis. Thus the tangent to the reference line at its beginning is $\mathbf{t}_z(0)$, and at its end it is $\mathbf{t}_z(\theta)$. Futhermore, let z denote an arclength coordinate along this reference line, with $z = 0$ at the beginning of the reference line, and $z = l$ at the end of the reference line. The position vector of a point a distance z along the reference line will be denoted by

$$\mathbf{r} = \hat{\mathbf{r}}(z, l, \theta) \tag{A.2}$$

The unit tangent vector to the reference line pointing in the direction of increasing z can then be written as,

$$\hat{\mathbf{r}}_{,z} = \mathbf{t}_z\left(\frac{z\theta}{l}\right) \tag{A.3}$$

where a comma followed by a subscript denotes differentiation with respect to the variable appearing as a subscript. Finally a unit vector $\mathbf{t}_y = \mathbf{t}_y(\alpha)$ can be defined by the vector cross product as

$$\mathbf{t}_y(\alpha) = \mathbf{t}_z(\alpha) \times \mathbf{t}_x \tag{A.4}$$

Thus, for positive θ, $\mathbf{t}_y = \mathbf{t}_y(z\theta/l)$ is a unit vector lying in the plane of deformation, normal to the reference line, and pointing towards the convex side of the reference line. As a result of these definitions, $\mathbf{t}_x, \mathbf{t}_y$, and $\mathbf{t}_z$ form a proper orthonormal triad. It further follows from geometry that,

$$\mathbf{t}_y'(\alpha) = \mathbf{t}_z(\alpha), \qquad \mathbf{t}_z'(\alpha) = -\mathbf{t}_y(\alpha) \quad \forall\ \alpha \tag{A.5}$$

where a prime denotes differentiation with respect to the argument (i.e. with respect to the angle α). The position vector of an arbitrary point (x, y, z) can now be written as

$$\hat{\mathbf{p}}(x, y, z, t) = \hat{\mathbf{r}}(z, l(t), \theta(t)) + x\mathbf{t}_x + y\mathbf{t}_y\left(\frac{z\theta(t)}{l(t)}\right) \tag{A.6}$$

Thus the coordinates (x, y) define the location of the point under consideration on the cross-section, and z defines the location of the cross-section in terms of arclength distance along the reference line. Note that (x, y, z) represent curvilinear coordinates rather than the usual cartesian coordinates. Furthermore this curvilinear coordinate system is always orthogonal, but changes as a function of time, according to $l(t)$ and $\theta(t)$.

In order to describe the deformation of the system, consider first the undeformed configuration corresponding to time $t = 0$. Let L and Θ denote the values of l and θ before deformation. Thus

$$L = l(0), \quad \Theta = \theta(0) \tag{A.7}$$

For an initially straight beam segment, one would have $\Theta = 0$ and L would be the initial length of the beam segment. (Generally upper case symbols will be used for the undeformed configuration and lower case symbols for the deformed configuration.) The position vector of a point (X, Y, Z) before deformation can be written as

$$\mathbf{P}(X, Y, Z) = \hat{\mathbf{p}}(X, Y, Z, 0) = \hat{\mathbf{r}}(Z, L, \Theta) + X\mathbf{t}_x + Y\mathbf{t}_y\left(\frac{Z\Theta}{L}\right) \tag{A.8}$$

Thus the coordinates (X, Y, Z) label a material point before deformation. The position vector of the same material point after a uniform deformation can be defined by Eq. (A.6) with

$$x = X + u(X, Y, t), \qquad y = Y + v(X, Y, t), \qquad z = Zl(t)/L \tag{A.9}$$

$$l(t) = L + W(t), \qquad \theta(t) = \Theta + \phi(t) \tag{A.10}$$

where $u = u(X, Y, t)$ and $v = v(X, Y, t)$ are cross-sectional displacement components that describe the distortion of the cross-section, $W(t)$ represents the elongation of the reference line, and $\phi(t)$ is the rotation at the end of the beam. The coordinates (X, Y, Z) provide a label for a specific material point. By substituting Eqs. (A.9) and (A.10) into Eq. (A.6), this position vector of the same material point (X, Y, Z) after deformation can then be written as

$$\mathbf{p}(X, Y, Z, t) = \hat{\mathbf{r}}\left(\frac{Zl(t)}{L}, L + W(t), \Theta + \phi(t)\right) + (X + u(X, Y, t))\mathbf{t}_x + (Y + v(X, Y, t))\mathbf{t}_y\left(\frac{Z}{L}\theta(t)\right) \tag{A.11}$$

The above fully defines the deformation in terms of the cross-sectional displacements $u = u(X, Y, t)$ and $v = v(X, Y, t)$ in the x and y directions respectively, the elongation of the reference line $W = W(t)$, and the end rotation $\phi = \phi(t)$.

For the discretisation, a two-dimensional finite element mesh is used in the x–y plane, to interpolate the displacements u and v between nodal values of these displacements, and in addition an extra node is introduced, for which the degrees of freedom are W and ϕ, and the coordinates are L and Θ. All elements are attached to this same node, as well as being attached to each other in the usual way.

The deformation gradient tensor can be written as

$$\mathbf{F} = \mathbf{p}_{,X}\mathbf{T}_x + \mathbf{p}_{,Y}\mathbf{T}_y + \mathbf{p}_{,Z}(L/A_z)\mathbf{T}_z \tag{A.12}$$

where

$$\mathbf{T}_x = \mathbf{t}_x, \quad \mathbf{T}_y = \mathbf{t}_y(\Theta Z/L), \quad \mathbf{T}_z = \mathbf{t}_z(\Theta Z/L) \tag{A.13}$$

are the unit vectors $\mathbf{t}_x$, $\mathbf{t}_y$, $\mathbf{t}_z$ for the undeformed configuration and,

$$A_z = L\|\mathbf{P}_{,Z}\| = L + Y\Theta \tag{A.14}$$

is the undeformed length of a fibre of the beam.

The Green–Lagrange strain tensor is given by,

$$\mathbf{E} = \tfrac{1}{2}(\mathbf{F}^{\mathrm{T}} \cdot \mathbf{F} - \mathbf{1}) \tag{A.15}$$

where $\mathbf{1}$ represents the unit tensor. Evaluating this yields,

$$\mathbf{E} = E_{xx}\mathbf{T}_x\mathbf{T}_x + E_{yy}\mathbf{T}_y\mathbf{T}_y + E_{xy}(\mathbf{T}_x\mathbf{T}_y + \mathbf{T}_y\mathbf{T}_x) + E_{zz}\mathbf{T}_z\mathbf{T}_z \tag{A.16}$$

where

$$E_{xx} = u_{,X} + \tfrac{1}{2}(u_{,X}^2 + v_{,X}^2) \tag{A.17}$$

$$E_{yy} = v_{,Y} + \tfrac{1}{2}(u_{,Y}^2 + v_{,Y}^2) \tag{A.18}$$

$$2E_{xy} = u_{,Y} + v_{,X} + u_{,X}u_{,Y} + v_{,X}v_{,Y} \tag{A.19}$$

$$E_{zz} = \varepsilon_z + \tfrac{1}{2}\varepsilon_z^2, \tag{A.20a}$$

$$\varepsilon_z = \frac{W + \Theta v + \phi(Y + v)}{A_z} \tag{A.20b}$$

The finite element procedures are derived directly by standard methods from these expressions for the strains, based on the principle of virtual displacements in the form,

$$\delta W = \int_{\Omega} (\tau^{xx}\delta E_{xx} + \tau^{yy}\delta E_{yy} + \tau^{zz}\delta E_{zz} + 2\tau^{xy}\delta E_{xy}) A_z \mathrm{d}X\mathrm{d}Y \tag{A.21}$$

in which δW denotes the virtual work performed by the applied loads; Ω denotes the undeformed cross-section; δE_{xx}, etc. are the virtual strains (variations in the strains E_{xx} etc. associated with the virtual displacement field); and τ^{xx} are the components of the second Piola Kirchhoff stress tensor given by

$$\mathbf{S} = \tau^{xx}\mathbf{T}_x\mathbf{T}_x + \tau^{yy}\mathbf{T}_y\mathbf{T}_y + \tau^{zz}\mathbf{T}_z\mathbf{T}_z + \tau^{xy}(\mathbf{T}_x\mathbf{T}_y + \mathbf{T}_y\mathbf{T}_x) \tag{A.22}$$

Note that the virtual work integral has been reduced to an integral over the undeformed cross-section Ω, since the strain components are not a function of the axial coordinate Z.

The discretisation used in the analyses reported herein is based on the 4-node isoparametric element with a single integration point at its centre and hourglass control such as described in Belytschko and Ong, 1984. The amount of hourglass control used was such that the bending stiffness of a square element would be 0.1% of the correct stiffness in the elastic range. It was also verified for some examples that changing this hourglass control stiffness by a factor of 10 did not produce significant changes in the results.

A.2. Bifurcation check

For the prebuckling solution, the only needed displacement components were the cross-sectional displacements $u = u(X, Y, t)$ and $v = v(X, Y, t)$, and the "displacements" describing the change in length and curvature of the beam, $W = W(t)$ and $\phi = \phi(t)$, respectively. For the bifurcation check, however, a more general displacement field needs to be considered. For this purpose, the cross-sectional displacements u and v are also allowed to vary as a function of the axial coordinate Z, and an axial displacement $w = w(X, Y, Z, t)$ needs to be introduced. Thus for a general deformation, the position vector of a material point (X, Y, Z) after deformation can be written as,

$$\mathbf{p}(X, Y, Z, t) = \hat{\mathbf{r}}\left(\frac{Zl}{L}, l, \theta\right) + (X + u)\mathbf{t}_x + (Y + v)\mathbf{t}_y\left(\frac{Z\theta}{L}\right) + w\mathbf{t}_z\left(\frac{Z\theta}{L}\right) \tag{A.23}$$

where now

$$u = u(X, Y, Z, t), \quad v = (X, Y, Z, t), \quad w = w(X, Y, Z, t) \tag{A.24}$$

Note that Eq. (A.23) now supersedes Eq. (A.11), since Eq. (A.11) describes a deformation that is uniform along the length of the beam, whereas Eq. (A.23) describes a fully general deformation. This means that all previous results relying on Eq. (A.11) are no longer applicable. Indeed of the previous results, only Eqs. (A.1)–(A.8), (A.10), (A.12) and (A.13)–(A.15) still apply. The others need to be re-derived for the more general deformation of Eq. (A.23). Proceeding in a similar way as before, but with the more general deformation gives

$$\mathbf{E} = E_{xx}\mathbf{T}_x\mathbf{T}_x + E_{yy}\mathbf{T}_y\mathbf{T}_y + E_{zz}\mathbf{T}_z\mathbf{T}_z + E_{xy}(\mathbf{T}_x\mathbf{T}_y + \mathbf{T}_y\mathbf{T}_x) + E_{xz}(\mathbf{T}_x\mathbf{T}_z + \mathbf{T}_z\mathbf{T}_x) + E_{yz}(\mathbf{T}_y\mathbf{T}_z + \mathbf{T}_z\mathbf{T}_y) \tag{A.25}$$

for the Green–Lagrange strain tensor, in which

$$E_{xx} = u_{,X} + \tfrac{1}{2}(u_{,X}^2 + v_{,X}^2 + w_{,X}^2) \tag{A.26}$$

$$E_{yy} = v_{,Y} + \tfrac{1}{2}(u_{,Y}^2 + v_{,Y}^2 + w_{,Y}^2) \tag{A.27}$$

$$E_{zz} = \frac{L^2}{A_z^2}\left\{u_{,Z}^2 + \left(v_{,Z} - \frac{\theta}{L}w\right)^2 + \left(\frac{a_z}{L} + w_{,Z}\right)^2 - \frac{A_z^2}{L^2}\right\} \tag{A.28}$$

$$2E_{xy} = u_{,Y} + v_{,X} + u_{,X}u_{,Y} + v_{,X}v_{,Y} + w_{,X}w_{,Y} \tag{A.29}$$

$$2E_{xz} = \frac{L}{A_z}\left\{(1+u_{,X})u_{,Z} + v_{,X}\left(v_{,Z} - \frac{\theta}{L}w\right) + w_{,Y}\left(\frac{a_Z}{L} + w_{,Z}\right)\right\} \tag{A.30}$$

$$2E_{yz} = \frac{L}{A_z}\left\{u_{,Y}u_{,Z} + (1+v_{,y})\left(v_{,Z} - \frac{\theta}{L}w\right) + w_{,Y}\left(\frac{a_Z}{L} + w_{,Z}\right)\right\} \tag{A.31}$$

where

$$a_z = l + \theta y = L + W + (\Theta + \phi)(Y + v) \tag{A.32}$$

The variational form of the bifurcation condition can be written as (Hutchinson, 1974)

$$\delta\tilde{W} = \int_\Omega \int_0^L (L^{ijkl}\tilde{E}_{kl}\delta E_{ij} + \tau^{ij}\delta\tilde{E}_{ij})\frac{A_z}{L}\mathrm{d}Z\,\mathrm{d}X\,\mathrm{d}Y \tag{A.33}$$

in which summation over repeated indecies i, j, k and l is implied with each index taking a value "x", "y", or "z"; W denotes the work done by the applied loads; E_{ij} and τ^{ij} are the components of the Green–Lagrange strain tensor and the second Piola–Kirchhoff stress tensor, respectively, as before; a δ or a tilde applied to any entity $(\cdot)$ denotes a variation with respect to the displacement field $\mathbf{u}$ as in

$$\delta(\cdot) = (\cdot)_{,\mathbf{u}}\delta\mathbf{u}, \quad \tilde{(\cdot)} = (\cdot)_{,\mathbf{u}}\tilde{\mathbf{u}}, \quad \delta\tilde{(\cdot)} = (\cdot)_{,\mathbf{uu}}\tilde{\mathbf{u}}\,\delta\mathbf{u} \tag{A.34}$$

in which $(\cdot)_{,\mathbf{u}}$ denotes a Frećhet derivative (or variation) of the quantity $(\cdot)$ with respect to the displacement field; $\delta\mathbf{u}$ denotes the virtual displacement field; $\tilde{\mathbf{u}}$ denotes the displacement field associated with the buckling mode; and L^{ijkl} are the incremental (tangent) moduli (as in $\dot{\tau}^{ij} = L^{ijkl}\dot{E}_{kl}$, where a dot denotes the time-derivative) based on the assumption that plastic loading occurs wherever plastic loading occurs for load increments on the prebuckling solution path.

In general, the incremental moduli used in the bifurcation condition (Eq. (A.33)) should be the ones that apply for the prebuckling solution under increasing applied load. However here the bifurcation check is based on the L^{ijkl} of deformation theory of plasticity, whereas the flow theory of plasticity is used for the prebuckling solution. The incremental moduli for both theories may be obtained from Needleman and Tvergaard (1977) [4]. The reason for using the incremental moduli of the deformation theory for the bifurcation check is that this has been found to give better agreement with the experimental observations of bifurcation buckling.

To evaluate the strain components and relevant variations of the strains in Eq. (A.23), the following expressions for the buckling mode, and the virtual displacement field are used,

$$\tilde{\mathbf{u}}(X,Y,Z) = \tilde{u}(X,Y)\cos(kZ)\mathbf{t}_x + \tilde{v}(X,Y)\cos(kZ)\mathbf{t}_y\left(\frac{Z}{L}\theta\right) + \tilde{w}(X,Y)\sin(kZ)\mathbf{t}_z\left(\frac{Z}{L}\theta\right) \tag{A.35}$$

$$\delta\mathbf{u}(X,Y,Z) = \delta u(X,Y)\cos(kZ)\mathbf{t}_x + \delta v(X,Y)\cos(kZ)\mathbf{t}_y\left(\frac{Z}{L}\theta\right) + \delta w(X,Y)\sin(kZ)\mathbf{t}_z\left(\frac{Z}{L}\theta\right) + \mathrm{OT} \tag{A.36}$$

in which OT denotes "orthogonal terms" which vanish upon integration with respect to Z in Eq. (A.32); and k is the wave number of the buckling mode (with respect to undeformed length along the reference

[4] Note, however, that some translation of notation is required, because here L^{ijkl} denotes the components of a 4th-order tensor relating the convective rate of the Kirchhoff stress tensor to the rate of deformation tensor, which is not the same as what Needleman and Tvergaard (1977) denote by L^{ijkl}.

line). Thus the buckling mode is defined by the displacement fields $\tilde{u} = \tilde{u}(X, Y)$, $\tilde{v} = \tilde{v}(X, Y)$ and $\tilde{w}(X, Y)$, and by the wave number k.

The wave number can be written as

$$k = \frac{n\pi}{L} \tag{A.37}$$

where n is the number of half wavelengths within the length of beam considered. For an integer value of n, the buckling mode is consistent with symmetry boundary conditions at both ends of the beam. For the purpose of evaluating the integral in Eq. (A.32) with respect to Z, an integer value of n is assumed. However, if end effects are not important, and one is interested in the critical buckling modes within a long beam, one can use the same finite element formulation developed here with any value of L, and find the wave number k for which the bifurcation occurs first, without restricting oneself to values of k given by Eq. (A.36) for integer values of n.

Evaluating the variations of the strain components according to Eq. (A.33) gives,

$$\delta E_{xx} = \{(1 + u_{,X})\delta u_{,X} + v_{,x}\delta v_{,X}\}\cos(kZ) \tag{A.38}$$

$$\delta E_{yy} = \{u_{,Y}\delta u_{,Y} + (1 + v_{,Y})\delta v_{,Y}\}\cos(kZ) \tag{A.39}$$

$$\delta E_{zz} = \left(\frac{L}{A_z}\right)^2 \frac{a_z}{L}\left(k\delta w + \frac{\theta}{L}\delta v\right)\cos(kZ) \tag{A.40}$$

$$2\delta E_{xy} = \{(1 + u_{,X})\delta u_{,Y} + v_{,X}\delta v_{,Y} + u_{,Y}\delta u_{,X} + (1 + v_{,Y})\delta v_{,X}\}\cos(kZ) \tag{A.41}$$

$$2\delta E_{xz} = \frac{L}{A_z}\left\{ - (1 + u_{,X})k\delta u - v_{,X}\left(k\delta v + \frac{\theta}{L}\delta w\right) + \frac{a_z}{L}\delta w_{,X}\right\}\sin(kZ) \tag{A.42}$$

$$2\delta E_{yz} = \frac{L}{A_z}\left\{ - u_{,Y}k\delta u - (1 + v_{,Y})\left(k\delta v + \frac{\theta}{L}\delta w\right) + \frac{a_z}{L}\delta w_{,Y}\right\}\sin(kZ) \tag{A.43}$$

in which $u = u(X, Y)$ and $v = v(X, Y)$ are the prebuckling displacements; the derivative with respect to the coordinates X and Y are denoted by $(\cdot)_{,X}$ and $(\cdot)_{,Y}$ respectively; A_z is given by Eq. (A.14), and a_z by Eq. (A.32).

The quantities $\tilde{E}_{ij}$ (linearised strain increments associated with the buckling mode) may also be calculated from Eqs. (A.37)–(A.42), by replacing δu, δv and δw by $\tilde{u}$, $\tilde{v}$ and $\tilde{w}$, respectively. Finally for the second variations of the strain components E_{ij} with respect to the displacements one obtains,

$$\int_0^L \delta\tilde{E}_{xx}\mathrm{d}Z = \frac{L}{2}\left\{\tilde{u}_{,X}\delta u_{,X} + \tilde{v}_{,X}\delta v_{,X} + \tilde{w}_{,X}\delta w_{,X}\right\} \tag{A.44}$$

$$\int_0^L \delta\tilde{E}_{yy}\mathrm{d}Z = \frac{L}{2}\{\tilde{u}_{,Y}\delta u_{,Y} + \tilde{v}_{,Y}\delta v_{,Y} + \tilde{w}_{,Y}\delta w_{,Y}\} \tag{A.45}$$

$$\int_0^L \delta\tilde{E}_{zz}\mathrm{d}Z = \frac{L}{2}\left(\frac{L}{A_z}\right)^2\left\{k^2\delta u\tilde{u} + \left(k\delta v + \frac{\theta}{L}\delta w\right)\left(k\tilde{v} + \frac{\theta}{L}\tilde{w}\right) + \left(k\delta w + \frac{\theta}{L}\delta v\right)\left(k\tilde{w} + \frac{\theta}{L}\tilde{v}\right)\right\} \tag{A.46}$$

$$\int_0^L 2\delta\tilde{E}_{xy}dZ = \frac{L}{2}\{\delta u_{,X}\tilde{u}_{,Y} + \tilde{u}_{,X}\delta u_{,Y} + \delta v_{,X}\tilde{v}_{,Y} + \tilde{v}_{,X}\delta v_{,Y} + \delta w_{,X}\tilde{w}_{,Y} + \tilde{w}_{,X}\delta w_{,Y}\} \tag{A.47}$$

$$\int_0^L \delta\tilde{E}_{xz}\mathrm{d}Z = \int_0^L \delta\tilde{E}_{yz}\mathrm{d}Z = 0 \tag{A.48}$$

Using the interpolation scheme of the two-dimensional finite element discretisation of the cross-section to define the buckling mode displacements $\tilde{u} = \tilde{u}(X, Y)$, $\tilde{v} = \tilde{v}(X, Y)$, and $\tilde{w} = \tilde{w}(X, Y)$ in terms of nodal values of the buckling mode displacements, proceeding in a similar manner for the virtual displacements $\delta u = \delta u(X, Y)$, $\delta v = \delta v(X, Y)$ and $\delta w = \delta w(X, Y)$, and substituting these expressions for the strain variations into the variational form of the bifurcation condition (Eq. (A.33)), one obtains the stability condition in the usual matrix form.

Note that three degrees of freedom per node are involved for the stability check, as opposed to two for the prebuckling solution. On the other hand, the buckling mode does not involve deformations of the reference line, so that the degrees of freedom associated with the deformations of the reference line (displacements W and ϕ of the extra node) are not needed for the bifurcation check.

The OT in Eq. (A.36) deserve some comment. These represent virtual displacements fields that can be written in the same form of Eq. (A.36), but for a value of the wave number k corresponding to a different integer n in Eq. (A.37). By adding such terms one can represent any admissible virtual displacement field, yet the contribution of such terms vanishes upon integration with respect to Z in Eq. (A.32). As a result the variational bifurcation condition is satisfied not just for virtual displacements with the same sort of sinusoidal variation as the buckling mode, but for any admissible virtual displacement. This means that the exact buckling mode is indeed in the form of Eq. (A.34). i.e. the form of sinusoidal variations of the buckling mode chosen is not an approximation, but rather the exact solution. The only approximation is due to the discretisation of the cross-section.

With a method to calculate the stability matrix in place, one still needs a practical strategy of finding the bifurcation point, i.e. the point where the stability matrix first loses the positive definite property. For this purpose, the stability matrix is evaluated at each loadstep of the prebuckling solution for various values of the wave number k, and checked for any negative eigenvalues. (In this context a "loadstep" means a converged solution to the prebuckling problem.) Once a negative eigenvalue is detected during the factorisation of the stability matrix, the minimum eigenvalue of the stability matrix for each wave number is calculated, in order to generate a plot of the minimum eigenvalue as a function of the wave number k (or as a function of the logarithm of the wave number). The minimum of this plot can be found by interpolating with a parabola, fitted to the lowest point on this plot and the adjacent points to each side. The critical wave number and the interpolated minimum eigenvalue are then determined from the point where this parabola reaches a minimum value. This calculation is repeated for the loadsteps that straddle the bifurcation point. (i.e. the point where the interpolated minimum eigenvalue is zero.) Finally one can use linear interpolation between the straddling loadsteps to determine the interpolated location of the bifurcation point. If necessary one can improve the approximation, by restarting the analysis, and calculating the eigenvalues of the stability matrix for more densely spaced values of the wave number and/or for smaller load increments of the prebuckling solution.

In the calculations reported in this paper, the increment in the nominal bending strain at each loadstep was 0.01%, and the wave numbers for which the stability matrix was evaluated differed by 10% or less (using evenly spaced values of the logarithm of the wave number, and assuming for the purpose of interpolation that the minimum eigenvalue of the stability matrix is a quadratic function of the logarithm of the wave number). Under such conditions refinement of the search for the critical bifurcation point is not considered necessary.

References

Bai, Y., Igland, R., Moan, T., 1995. Collapse of thick tubes under combined tension and bending. J. Construct. Steel Res. 32, 233–257.
Batdorf, S.B., 1949. Theories of plastic buckling. J. Aero. Sci. 16, 405.
Batterman, S.C., 1965. Plastic buckling of axially compressed cylindrical shells. AIAA J. 3 (2), 316–325.

Batterman, S.C., 1967. Tangent modulus theory for cylindrical shells: buckling under increasing load. Int. J. Solids Struct. 3, 501–512.
Belytschko, T., Ong, J.S.J., 1984. Hourglass control in linear and nonlinear problems. Comput. Meth. Appl. Mech. Engng. 43, 251–276.
Blachut, J., Galletly, G.D., James, S., 1996. On the plastic buckling paradox for cylindrical shells. Proc. Inst. Mech. Engrs. 210, 477.
Boussaa, D., Dang Van, K., Labbé, P., Tang, H., 1995. Axisymmetric elastic–plastic FE analysis of pressurized elbows. J. Pressure Vessel Technol. 117 (4), 357–364.
Boussaa, D., Dang Van, K., Labbé, P., Tang, H.T., 1996. Finite pure bending of curved pipes. Comput. Struct. 60 (6), 1003–1012.
Bushnell, D., 1982. Plastic buckling. In: S.Y. Zamrik, D. Dietrich (Eds.), Pressure Vessels and Piping: Design Technology 1982, a Decade of Progress, ASME, NY Book No. G00213, pp. 47–117.
Christofersen, J., Hutchinson, J.W., 1979. A class of phenomenological corner theories of plasticity. J. Mech. Phys. Solids 27, 465–487.
Cook, R.D., 1989. Axisymmetric finite element analysis for pure moment loading of curved beams and pipe bends. Comput. Struct. 33 (2), 483–487.
Hecker, S.S., 1976. Experimental studies of yield phenomena in biaxially loaded metals, constitutive equations in viscoplasticity. AMD-vol. 20, ASME, New York, pp. 1–33.
HKS, 1989. ABAQUS Theory Manual. Hibbitt, Karlsson, and Sorensen, Pawtucket, Rhode Island, USA.
Hutchinson, J.W., 1974. Advances in Applied Mechanics, vol. 14, Academic Press, New York, p. 67.
Jirsa, J.O., Lee, F.H., Wilhoit, J.C., Fr., Merwin, J.E., 1972. Ovaling of pipelines under pure bending. Fourth Annual Offshore Technology Conference (OTC 1972), Houston, TX, May 1–3, Paper No. OTC 1569, vol. I, pp. 573–578.
Ju, G.T., Kyriakides, S., 1992. Bifurcation and localization instabilities in cylindrical shells under bending – II. predictions.. Int. J. Solids Struct. 29 (9), 1143–1171.
Kyriakides, S., Ju, G.T., 1992. Bifurcation and localization instabilities in cylindrical shells under bending – I. experiments.. Int. J. Solids Struct. 29 (9), 1117–1142.
Murphy, C.E., Langner, C.G., 1985. Ultimate pipe strength under bending, collapse and fatigue. Proc. 4th Int. Conf. Offshore Mech. Arctic Engng. (OMAE '85), vol. 1, Dallas, February 1985, pp. 467–477.
Needleman, A., Tvergaard, V., 1977. Necking of biaxially stretched elastic–plastic circular plates. J. Mech. Phys. Solids 25, 159–183.
Needleman, A., Tvergaard, V., 1982. Aspects of plastic post-buckling behaviour. In: Hopkins H.G., Sewell M.J. (Eds.), Mechanics of Solids, The Rodney Hill 60th Anniversary Volume, London, Pergamon Press, pp. 453–498.
Peek, R., 2000. Axisymmetric wrinkling of cylinders with finite strain. J. Engng. Mech. 26 (5), 455–461.
Reddy, B.D., 1979. An experimental study of the plastic buckling of circular cylinders in pure bending. Int. J. Solids Struct. 15, 669–683.
Sanders, J.L., 1954. Plastic stress–strain relations based on linear loading functions. Proceedings of the Second U.S. National Congress of Applied Mechanics, Ann Arbor, MI, 14–18 June 1954, edited by P.M. Naghdi, p. 445, American Soc. Mech. Engrs., New York.
Souza, L.T., Murray, D.W., 1994. Prediction of wrinkling behavior of girth-welded line pipe. Structual Engineering Report 197, Department of Civil Engineering, University of Alberta, Edmonton, Alberta, Canada T6G2G7.
Stören, S., Rice, J.R., 1975. Localized necking in thin sheets. J. Mech. Phys. Solids 23, 421–441.
Tang, S.C., Chu, C.C., Yeung, K.S., 1985. Collapse of long, noncircular, cylindrical shells under pure bending. Comput. Struct. 21 (6), 1345–1353.
Triantafyllidis, N., 1980. Bifurcation phenomena in pure bending. J. Mech. Phys. Solids 28, 221–245.
Tvergaard, V., 1983. Plastic buckling of axially compressed circular cylindrical shells. Thin-Walled Structures 1, 139–163.
Yoosef-Ghodsi, N., Kulak, G.L., Murray, D.W., 1994. Behavior of Girth-welded linepipe. Struct. Engng. Rep. no. 203, Department of Civil Engineering, University of Alberta, Edmonton, Alberta, Canada T6G2G7, September 1994.